Near-field magnetoabsorption of quantum dots

Constantinos Simserides,[1,2,*] Anna Zora,[1] and Georgios Triberis[1]
[1]*Physics Department, Solid State Section, University of Athens, Panepistimiopolis, Zografos, GR-15784, Athens, Greece*
[2]*Materials Science Department, University of Patras, Panepistimiopolis, Rio, GR-26504, Patras, Greece*
(Received 30 June 2005; revised manuscript received 19 December 2005; published 13 April 2006)

We investigate the effect of an external magnetic field of variable *orientation* and *magnitude* (up to 20 T) on the linear near-field optical absorption spectra of single and coupled III-V semiconductor quantum dots. We focus on the *spatial* as well as on the *magnetic confinement*, varying the dimensions of the quantum dots and the magnetic field. We show that the ground-state exciton binding energy can be manipulated utilizing the spatial and magnetic confinement. The effect of the magnetic field on the absorption spectra, increasing the near-field illumination spot, is also investigated. The zero-magnetic-field "structural" symmetry can be destroyed varying the magnetic field orientation and this affects the near-field spectra. The asymmetry induced (except for specific orientations along symmetry axes) by the magnetic field can be revealed in the near-field but not in the far-field spectra. We predict that near-field magnetoabsorption experiments, of realistic spatial resolution, will be in the position to bring to light the quantum dot symmetry. This exceptional *symmetry-resolving power* of the near-field magnetoabsorption is lost in the far field. The influence of the Coulomb interactions on the absorption spectra is also discussed. Finally, we show that certain modifications of the magnetoexcitonic structure can be uncovered using a realistically acute near-field probe of $\approx$20 nm.

DOI: 10.1103/PhysRevB.73.155313 PACS number(s): 73.21.La, 71.35.Cc, 71.35.Ji, 87.64.Xx

I. INTRODUCTION

According to the Rayleigh formulation of Abbe's criterion, the best resolution which can be obtained in the *far field*, in vacuum, using visible light, is $\approx$200 nm. From the early 1980s, the near-field scanning optical microscopy (NSOM or SNOM) has demolished this limit. NSOM stems from an idea proposed by Synge[1] in 1928. The illumination or the light collection is performed in a spot with dimensions smaller than the wavelength λ, but simultaneously, in order to surpass the "diffraction limit," the light source or the light detector is placed *very close* to the sample: the—mainly—exponentially decaying, evanescent *near field* instead of the propagating far field is exploited. The Heisenberg uncertainty principle can qualitatively explain the creation of evanescent and propagating waves in the vicinity of a tiny hole in a screen.[2,3]

A "near-field microwave microscope" with a resolution of $\sim\lambda/60$ ($\lambda=3$ cm) was already demonstrated[4] in 1972. Due to the obvious technical difficulties, a scanning near-field *optical* microscope appeared more than one decade later.[5,6] Among the numerous applications of SNOM variants we quote quantum dot spectroscopy and microscopy,[7] investigation of phospholipid monolayers,[8] identification of chemical compounds by vibrational spectroscopy,[9] single-molecule detection,[10] Raman imaging,[11] photocurrent excitation in semiconductors,[12] lithography,[13] magnetic imaging,[14] logic and functional operations,[15] and many more. Review articles which describe the physics, techniques, and applications of the near-field optics can be found in the literature.[16–20]

One of the attractive features of NSOM is that optical transitions which are far-field (FF) forbidden may become near-field (NF) visible.[21] Theoretical calculations have foreseen that the Coulomb interaction and the spatial interference of the exciton wave functions bring on extraordinary nonmonotonic features to the linear absorption spectra of single and coupled semiconductor quantum dots (QDs).[22,23] When the spatial resolution is close to the excitonic Bohr radius ρ, the intensity of these spectral features depends on the spatial resolution in a remarkably nonmonotonic way.[22] A spatial resolution of $\approx$12 nm in the visible range had already been achieved in the early 1990s (Ref. 24) (e.g., imaging of tiny Al letters on a glass substrate). However, in the case of semiconductor heterostructures, where the quantum states are "buried" below the surface, the undisputable spatial resolution achieved at the end of the 1990s was $\approx$100–200 nm. For GaAs, $\rho\approx 12$ nm and therefore no direct comparison between theory and experiment could be made at that time. To make possible such a comparison, at least three points could be improved: (1) The surface cap layer which causes 50–100 nm detrimental spacing between the QD excitonic states and the aperture of the NF probe could be decreased. (2) Experimentalists could select a semiconductor with greater ρ—e.g., InAs with $\rho\approx 38$ nm. (3) The spatial resolution of the NF probes had to be sharpened. These improvements were to a significant degree met recently.[25,26] A spatial resolution of 30 nm ($\approx\lambda/30$, $\lambda=930$ nm) in the photoluminescence imaging of self-assembled InAs QDs (Ref. 25) and successful real-space mapping of the center-of-mass wave functions of an exciton confined in a naturally occurring GaAs QD (Ref. 26) were achieved. This experimental progress[25,26] gave more impulse to theoretical calculations. Indeed, the NF spectra of excitons and biexcitons formed in QDs naturally occurring at interface fluctuations of GaAs-based quantum wells have been recently calculated.[27,28] Finally, a theoretical description of SNOM on macromolecules has been most recently released.[29] Analogous "violations" of the FF selection rules have also been predicted for quantum wires (QWRs).[30] In the case of QWRs, the strong influence of the Coulomb interactions had

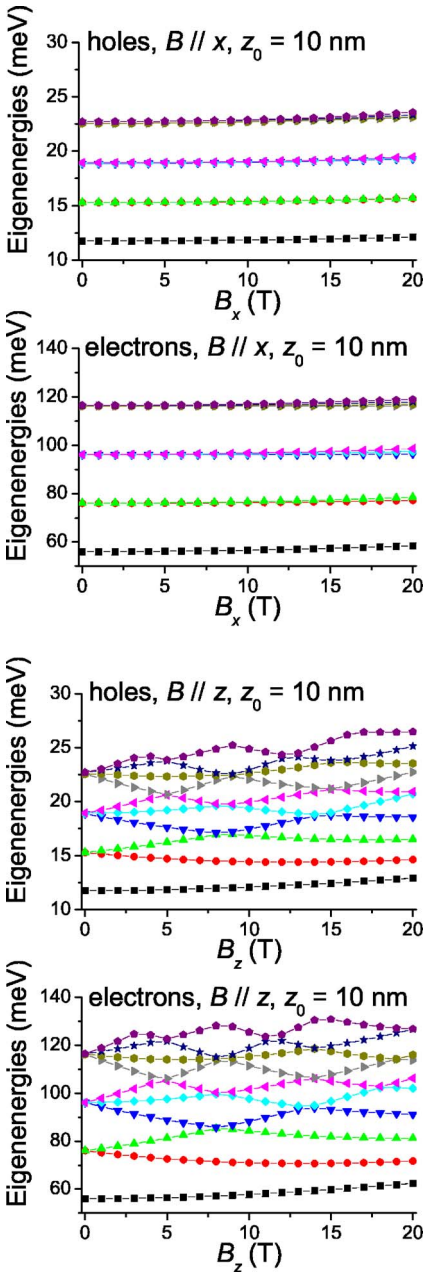

FIG. 1. (Color online) *Single quantum dot*, with QW width, z_0 =10 nm. Single-particle hole and electron eigenenergies as a function of B, applied in the x ($B\|x$) or in the z ($B\|z$) direction. The symmetry of these configurations is approximately ($B\|x$) or strictly ($B\|z$) cylindrical. Ten hole and ten electron eigenenergies are presented.

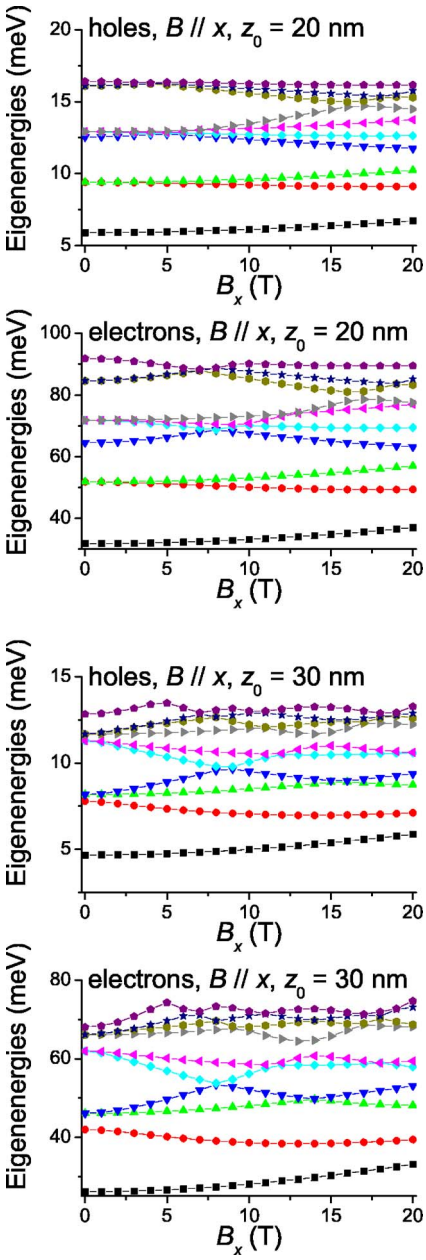

FIG. 2. (Color online) *Single quantum dots* with QW widths, z_0=20 nm and 30 nm. Single-particle hole and electron eigenenergies as a function of B, applied in the x ($B\|x$) direction. The zero-magnetic-field "structural" cylindrical symmetry has been broken by the "in-plane" magnetic field. Ten hole and ten electron eigenenergies are presented.

been demonstrated earlier by the quenching of the one-dimensional singularity in the single-particle density of states.[31]

The analysis of excitons in QDs subjected to a magnetic field $\boldsymbol{B}$ has been the subject of quite a few recent publications. We quote a theoretical description of excitons formed by N electrons and holes in InGaAs/GaAs QDs under a perpendicular magnetic field (single-particle Fock-Darwin spectrum).[32] We also cite a study of the effect of a perpendicular magnetic field, along the z axis, on the excitons of a QD with an asymmetric parabolic potential in the xy plane (with different harmonic oscillator frequencies along x and along y) and a narrow quantum well along the z axis,[33] as well as an investigation of the influence of a strong (up to 40 T) perpendicular magnetic field on the excitonic structure of a QD disk.[34] The NF method[22] allowed the identification of the corner and the side modes of the infrared spectra in triangular and square two-dimensional QDs which could be modified by a vertical magnetic field.[35] Preliminary calculations for a single QD, neglecting the Coulomb interaction,

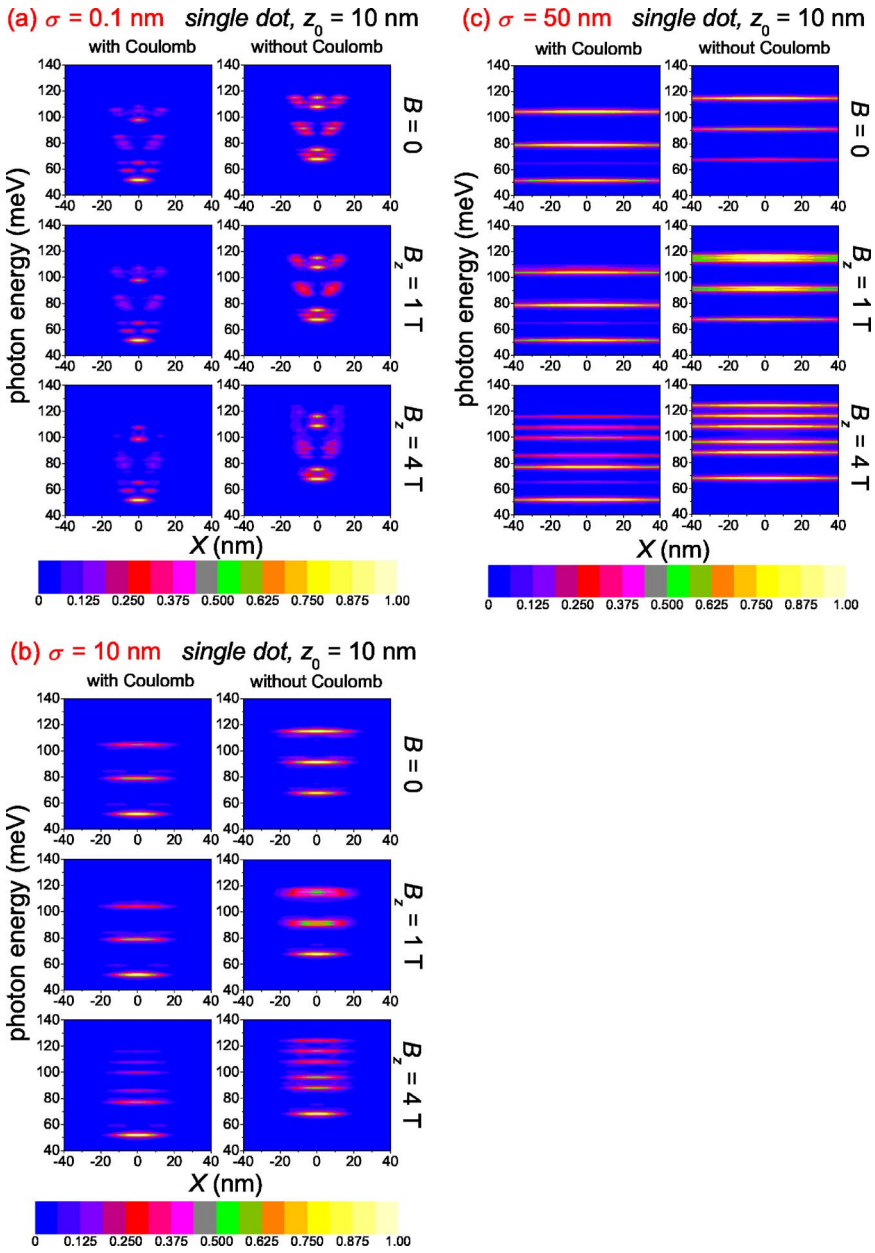

FIG. 3. (Color online) *Single quantum dot* with a square quantum well (z_0=10 nm) along the z axis and parabolic confinement in the xy plane. Local absorption $\alpha_\xi(X,\hbar\omega)$ (color scale) for different spatial resolutions $2\sqrt{2\ln 2}\sigma \approx 2.35\sigma$ *taking into account* or *neglecting* the Coulomb interactions. The structural (for B=0) cylindrical symmetry is preserved by the "perpendicular" magnetic field in this *ideal* configuration. X (nm) is the tip position along the x axis, while we keep Y=0. The photon energy $\hbar\omega$ (meV) is measured with respect to the band gap.

revealed interesting modifications of the absorption spectra under perpendicular magnetic field.[36]

In the works cited above,[32–36] $\boldsymbol{B}$ was applied in a characteristic perpendicular direction. Our computational scheme allows us to study QD structures of any given geometry, under a magnetic field of any orientation. In this framework we are not restricted to analytically solvable problems like the famous Fock-Darwin system. For B=0, the single QDs under study possess a "structural" cylindrical symmetry. However, we investigate the NF magnetoabsorption spectra under a "perpendicular" magnetic field which *conserves* and under an "in-plane" magnetic field which *destroys* this "structural" cylindrical symmetry. We explore the effect of the *spatial confinement* imposed by the QD dimensions and the *magnetic confinement* governed by $\boldsymbol{B}$. The single QDs considered here have a parabolic potential in the xy plane and a square quantum well (QW) in the z axis. We examine the effect of the spatial confinement varying the QW width (e.g., 10 nm, 20 nm, or 30 nm), while the magnetic confinement is modified changing the magnetic field orientation (e.g., along the z or x axis) and magnitude (0–20 T). Moreover, we consider the case of a double QD with a soft barrier. Increasing the illumination spot, we examine how $\boldsymbol{B}$ affects the calculated absorption spectra. The influence of the Coulomb interactions between electrons and holes is also discussed.

The article is organized in the following way: Our theoretical framework, consisting of four successive steps, is presented in Sec. II. First step (Sec. II A): calculation of the single-particle states of electrons and holes subjected to a magnetic field of variable magnitude and orientation, for a QD of arbitrary geometry. Second step (Sec. II B): computation of the Coulomb matrix elements for the interaction between electrons and holes. Third step (Sec. II C): evaluation of the excitonic eigenstates using the results obtained in Secs. II A and II B. Finally, Sec. II D (fourth step) summa-

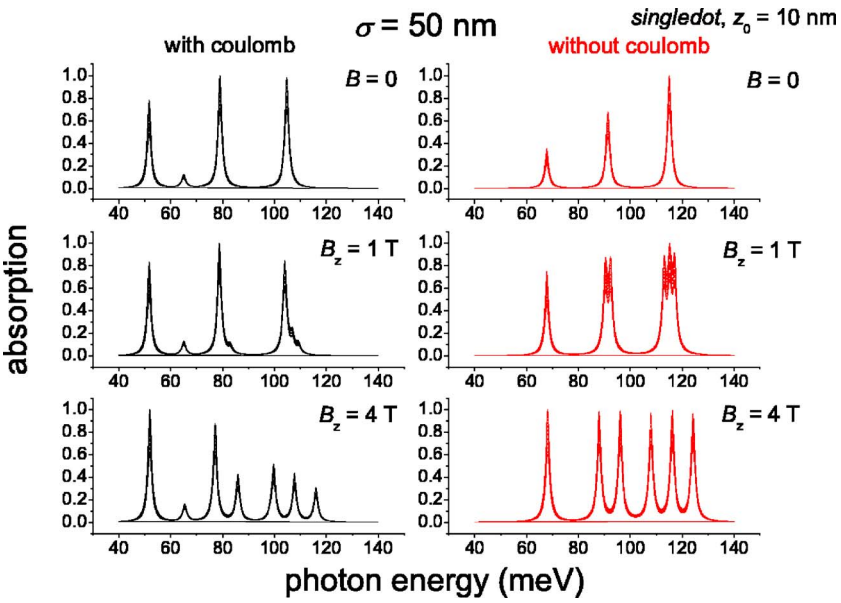

FIG. 4. (Color online) The "far-field" (σ=50 nm) absorption spectra of Fig. 3 as a function of the photon energy only—i.e., for all tip positions X.

rizes the necessary equations for the calculation of the NF absorption spectra. In Sec. III we show and discuss our results. Specifically, in Sec. III A we analyze the single-particle states of single QDs, focusing on the spatial confinement versus the magnetic field orientation and magnitude. In Sec. III B we concentrate on the magnetoabsorption of a single QD in an *ideal* configuration and we also discuss the influence of the Coulomb interactions. Furthermore, in Sec. III C we consider the magnetoabsorption of single QDs for higher values of B. The magnetic field orientation is also varied in order to emphasize its significance, especially in *symmetry breaking*. Moreover, in Sec. III D we analyze a double QD with a soft barrier. In addition, in Sec. III E we discuss the influence of the spatial and magnetic confinement on the ground-state exciton binding. Finally, we state our conclusions in Sec. IV.

The applicability of our method in actual experiments—i.e., the illumination of a nanostructure with a near-field probe in conjunction with the simultaneous application of an external magnetic field—may become a challenge to experimentalists. We hope that the results presented in this paper will encourage such an adventure.

II. THEORY

A. Single-particle states

We assume that the confining potential energy changes slowly enough, so that the envelope function approach is applicable. We also make the common hypothesis[32–35] that—since the energy region of interest is close to the semiconductor band gap—the effective-mass approximation with a single electron and hole band describes satisfactorily the band structure. A comprehensive comparison of the influence of the single-particle states calculation method (single-band effective-mass approximation, the multiband $\boldsymbol{k}\cdot\boldsymbol{p}$ method, and the tight-binding method) on the excitonic recombination spectrum in InAs/GaAs self-assembled quantum dots, without magnetic field, has been most recently published.[37] There, the authors establish to what extent the effective-mass approach is applicable to the description of the electronic states of self-assembled QDs by a systematic comparison of the above-stated calculation methods.[37]

We calculate the single-particle eigenstates of electrons and holes subjected to a magnetic field of variable orientation and under the three-dimensional QD confinement potential, imposed by the geometry and material parameters of the QD. We use an expansion into plane waves, $|\boldsymbol{k}\rangle$, within a periodicity box $\Omega=\mathcal{L}_x\mathcal{L}_y\mathcal{L}_z$. Accordingly, we expand the electron (or hole) envelope functions $|\phi^\mu\rangle$ into the orthonormal plane-wave basis $|\boldsymbol{k}\rangle$—i.e., $|\phi^\mu\rangle=\Sigma_{\boldsymbol{k}}C_{\boldsymbol{k}}^\mu|\boldsymbol{k}\rangle$. Due to the periodicity condition $k_{e/h,a}=\frac{2\pi n_a^{e/h}}{\mathcal{L}_a}$, where $n_a^{e/h}$ is an integer and $a=x,y,z$. The index h (e) denotes holes (electrons). The Hamiltonian is

$$\hat{H}=\frac{(\boldsymbol{p}-q\boldsymbol{A})^2}{2m^*}+U(\boldsymbol{r}). \tag{1}$$

$\boldsymbol{A}$ is the vector potential, and $U(\boldsymbol{r})$ is the confining potential energy. Notice that the spin is not taken into account in Eq. (1). Choosing $\boldsymbol{A}=\frac{\boldsymbol{B}\times\boldsymbol{r}}{2}$ and setting $q\boldsymbol{B}=\breve{\boldsymbol{B}}$, we find

$$\left\langle \boldsymbol{k}\left|\frac{(\boldsymbol{p}-q\boldsymbol{A})^2}{2m^*}\right|\boldsymbol{k}'\right\rangle=\frac{\hbar^2k'^2}{2m^*}\delta_{\boldsymbol{k}\boldsymbol{k}'}+\left\langle \boldsymbol{k}\left|\frac{\breve{B}^2r^2-(\breve{\boldsymbol{B}}\cdot\boldsymbol{r})^2}{8m^*}\right|\boldsymbol{k}'\right\rangle+\left\langle \boldsymbol{k}\left|\frac{-\breve{\boldsymbol{B}}\cdot\boldsymbol{L}}{2m^*}\right|\boldsymbol{k}'\right\rangle. \tag{2}$$

$\boldsymbol{L}$ is the angular momentum. Obviously,

$$\langle\boldsymbol{k}|U(\boldsymbol{r})|\boldsymbol{k}'\rangle=\frac{1}{\Omega}\int d^3\boldsymbol{r}\exp[-i(\boldsymbol{k}-\boldsymbol{k}')\cdot\boldsymbol{r}]U(\boldsymbol{r}). \tag{3}$$

We obtain the eigenenergies E^μ as well as the coefficients $C_{\boldsymbol{k}}^\mu$ by numerical diagonalization; i.e., we solve the following eigenvalue problem:

$$\sum_{k'} \{[\langle k|\hat{H}|k'\rangle - E^{\mu}\delta_k^{k'}]\langle k'|\phi^{\mu}\rangle\} = 0. \quad (4)$$

B. Coulomb matrix elements

Using the single-particle states, we calculate the Coulomb matrix elements $U^{eh}_{\mu\mu',\nu\nu'}$ between the different electron (μ,μ') and hole (ν,ν') states: specifically,

$$U^{eh}_{\mu\mu',\nu\nu'} = \int d^3\boldsymbol{r}_e \int d^3\boldsymbol{r}_h \phi^{\mu e*}(\boldsymbol{r}_e)\phi^{\mu' e}(\boldsymbol{r}_e)\frac{-e^2}{\kappa_0|\boldsymbol{r}_e-\boldsymbol{r}_h|} \times \phi^{\nu h*}(\boldsymbol{r}_h)\phi^{\nu' h}(\boldsymbol{r}_h) = U_{ll'}. \quad (5)$$

$l=\mu\nu$, $l'=\mu'\nu'$, and κ_0 is the dielectric constant. From Eq. (5) it is evident that the matrix $U_{ll'}$ is Hermitian. Setting $-\boldsymbol{q}_{e/h}=\boldsymbol{k}'_{e/h}-\boldsymbol{k}_{e/h}$, we obtain

$$U^{eh}_{\mu\mu',\nu\nu'} = \frac{-e^2}{\kappa_0}\sum_{\boldsymbol{q}_e,\boldsymbol{k}'_e,\boldsymbol{k}_h} C^{\mu^*}_{\boldsymbol{k}'_e+\boldsymbol{q}_e} C^{\mu'}_{\boldsymbol{k}'_e} C^{\nu^*}_{\boldsymbol{k}_h} C^{\nu'}_{\boldsymbol{k}_h+\boldsymbol{q}_e} \frac{4\pi}{q_e^2}. \quad (6)$$

C. Excitonic problem

The excitonic eigenvalue problem is the next step. We restrict ourselves to the linear optical regime; i.e., we assume that the system's dynamics are those of a single electron-hole pair. We expand the exciton eigenfunction in terms of single-particle envelope functions—i.e.,

$$\Psi^{\tau}(\boldsymbol{r}_e,\boldsymbol{r}_h) = \sum_{\mu\nu} \mathcal{C}^{\tau}_{\mu\nu}\phi^{\mu e}(\boldsymbol{r}_e)\phi^{\nu h}(\boldsymbol{r}_h). \quad (7)$$

The square modulus of $\Psi^{\tau}(\boldsymbol{r}_e,\boldsymbol{r}_h)$ is the probability of the electron being at the position $\boldsymbol{r}_e$ and the hole at the position $\boldsymbol{r}_h$. Accordingly, the excitonic eigenvalue problem, setting $\varpi_l=(E^{\mu e}+E^{\nu h})$, reads

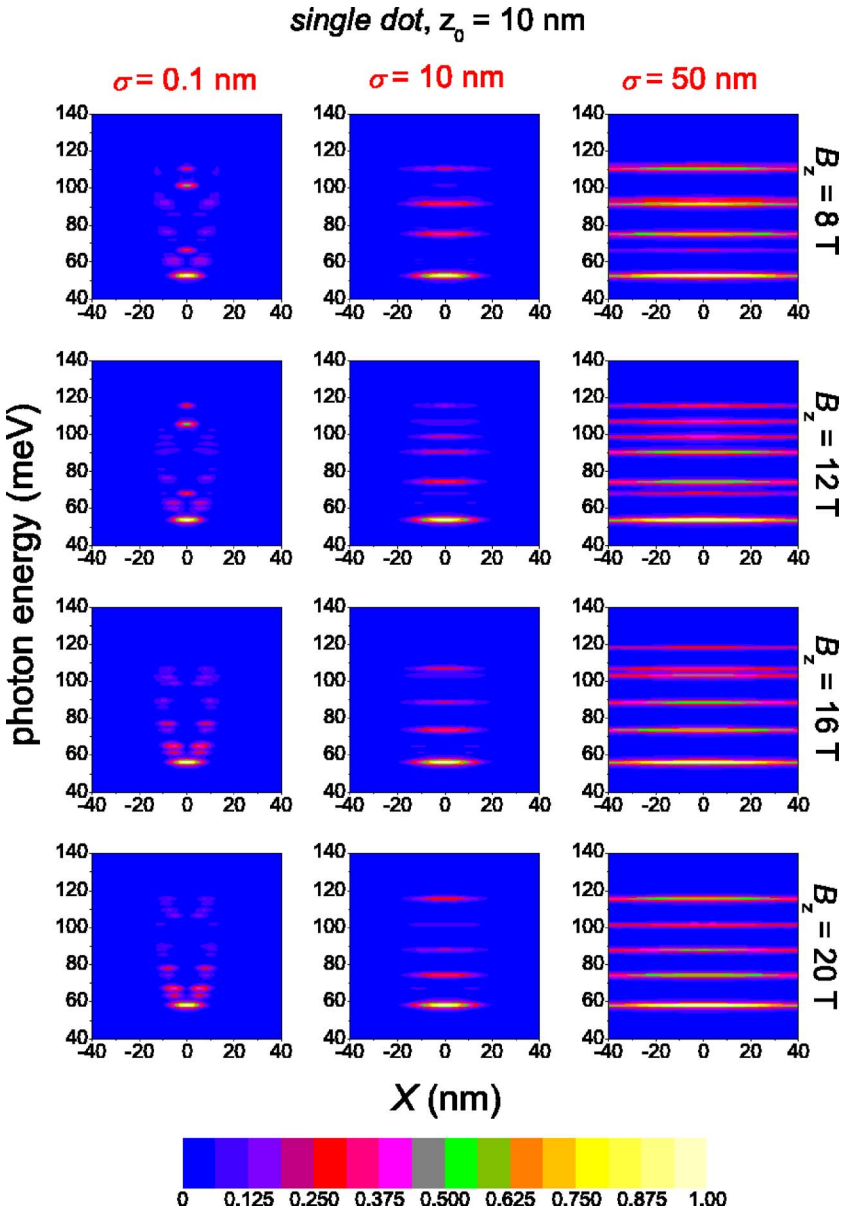

FIG. 5. (Color online) *Single quantum dot* with a square quantum well ($z_0=10$ nm) along the z axis and parabolic confinement in the xy plane. Local absorption $\alpha_{\xi}(X,\hbar\omega)$ (color scale) as a function of the tip position along the x axis, X (nm), and the photon energy measured with respect to the band gap, $\hbar\omega$ (meV). We keep $Y=0$. Each column corresponds to different spatial resolution $2\sqrt{2\ln 2}\sigma\approx 2.35\sigma$. Each row corresponds to a different value of the "perpendicular" magnetic field B_z. The "structural" (for $B=0$) cylindrical symmetry is preserved by the "perpendicular" magnetic field in this *ideal* configuration.

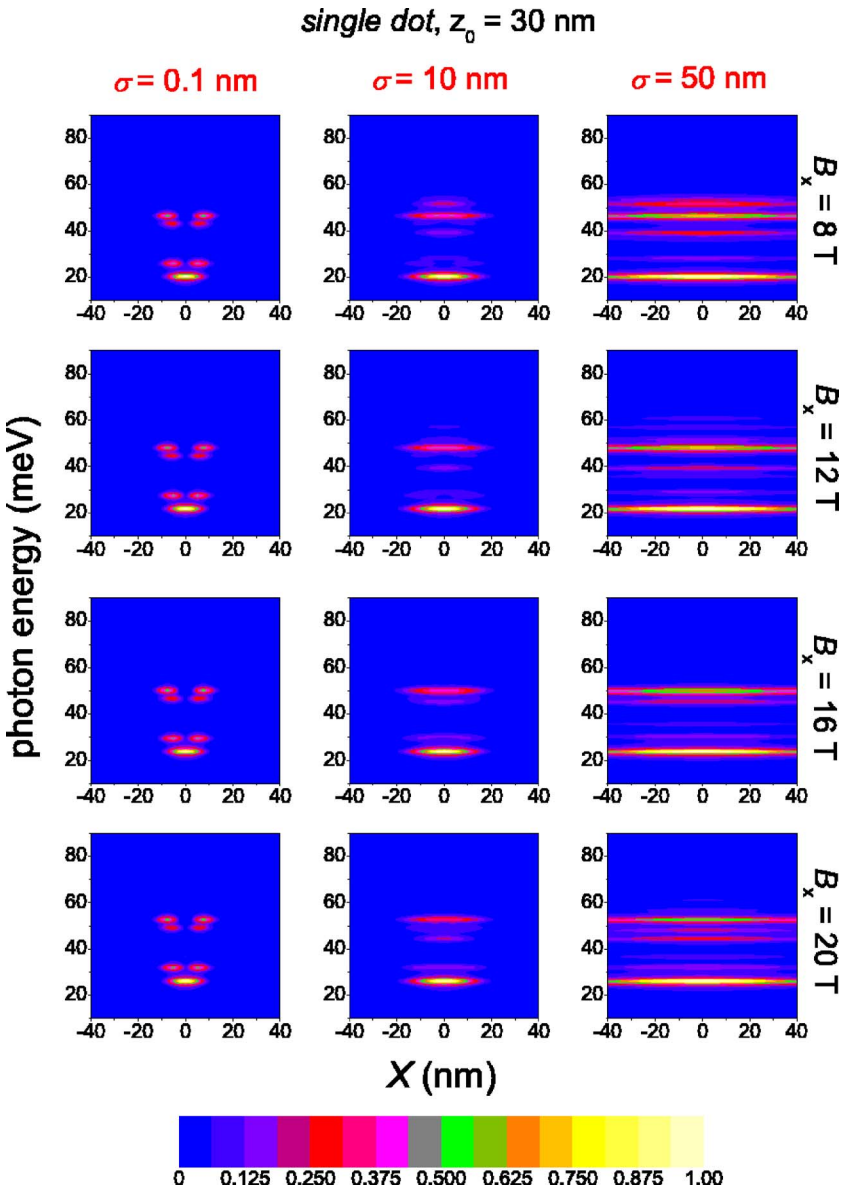

FIG. 6. (Color online) *Single quantum dot* with a square quantum well ($z_0=30$ nm) along the z axis and parabolic confinement in the xy plane. Local absorption $\alpha_\xi(X,\hbar\omega)$ (color scale) as a function of the tip position along the x axis, X (nm), and the photon energy measured with respect to the band gap, $\hbar\omega$ (meV). We keep $Y=0$. Each column corresponds to different spatial resolution, $2\sqrt{2\ln 2}\sigma \approx 2.35\sigma$. Each row corresponds to a different value of the "in-plane" magnetic field B_x. The zero-magnetic-field "structural" cylindrical symmetry has been broken by the "in-plane" magnetic field.

$$\sum_{l'} [\varpi_{l'}\delta_{ll'} + U_{ll'} - E^\tau \delta_{ll'}]\mathcal{C}^\tau_{l'} = 0. \tag{8}$$

Equation (8) is solved by numerical diagonalization. The excitonic matrix $S_{ll'}=\varpi_{l'}\delta_{ll'}+U_{ll'}$ is Hermitian in our regime of interest. The exciton eigenenergies E^τ give the energies, while the excitonic wave functions Ψ^τ give the oscillator strength of the optical transitions.

D. Near-field absorption spectra: Spatial resolution

Finally, we calculate the near-field optical absorption spectra. We suppose that the near-field illumination can be characterized by an electric field distribution $\mathcal{E}_\omega(\boldsymbol{r})$ with a given profile ξ centered around the beam position $\boldsymbol{R}$—i.e., that $\mathcal{E}_\omega(\boldsymbol{r})=\mathcal{E}_\omega\xi(\boldsymbol{r}-\boldsymbol{R})$. $\hbar\omega$ is the photon energy. We further suppose that $\mathcal{E}_\omega(\boldsymbol{r})$ is not affected from the static external magnetic field $\boldsymbol{B}$. This hypothesis is underpinned by NSOM's significant signal strength.[24] The local absorption for a given tip position, $\boldsymbol{R}$, is then expressed in the form[22]

$$\alpha_\xi(\boldsymbol{R},\omega) \propto \mathrm{Im}\sum_\tau \frac{\alpha^\tau_\xi(\boldsymbol{R})}{E^\tau - i\gamma - \hbar\omega}. \tag{9}$$

Here γ is a small damping constant, while $\alpha^\tau_\xi(\boldsymbol{R}) = |\int d^3\boldsymbol{r}\Psi^\tau(\boldsymbol{r},\boldsymbol{r})\xi(\boldsymbol{r}-\boldsymbol{R})|^2$. This means that, generally, for a narrow but finite probe, $\Psi^\tau(\boldsymbol{r},\boldsymbol{r})$ is averaged over a region which is determined by the spatial extension of the electric field profile. This is the *desired* experimental near-field situation. Under these circumstances, it has been shown[21,22] that excitonic transitions which are forbidden in the far field[38] may become visible in the near field. For the electric field profile we use $\xi(x,y,z)\propto\exp\left(-\frac{x^2+y^2}{2\sigma^2}\right)$. This implies that the hypothetical experimental situation is such that the probe is scanned parallel to the xy plane. The spatial resolution—i.e., the magnitude of the spot illuminated by the near-field probe—is then approximately given by the full width at half

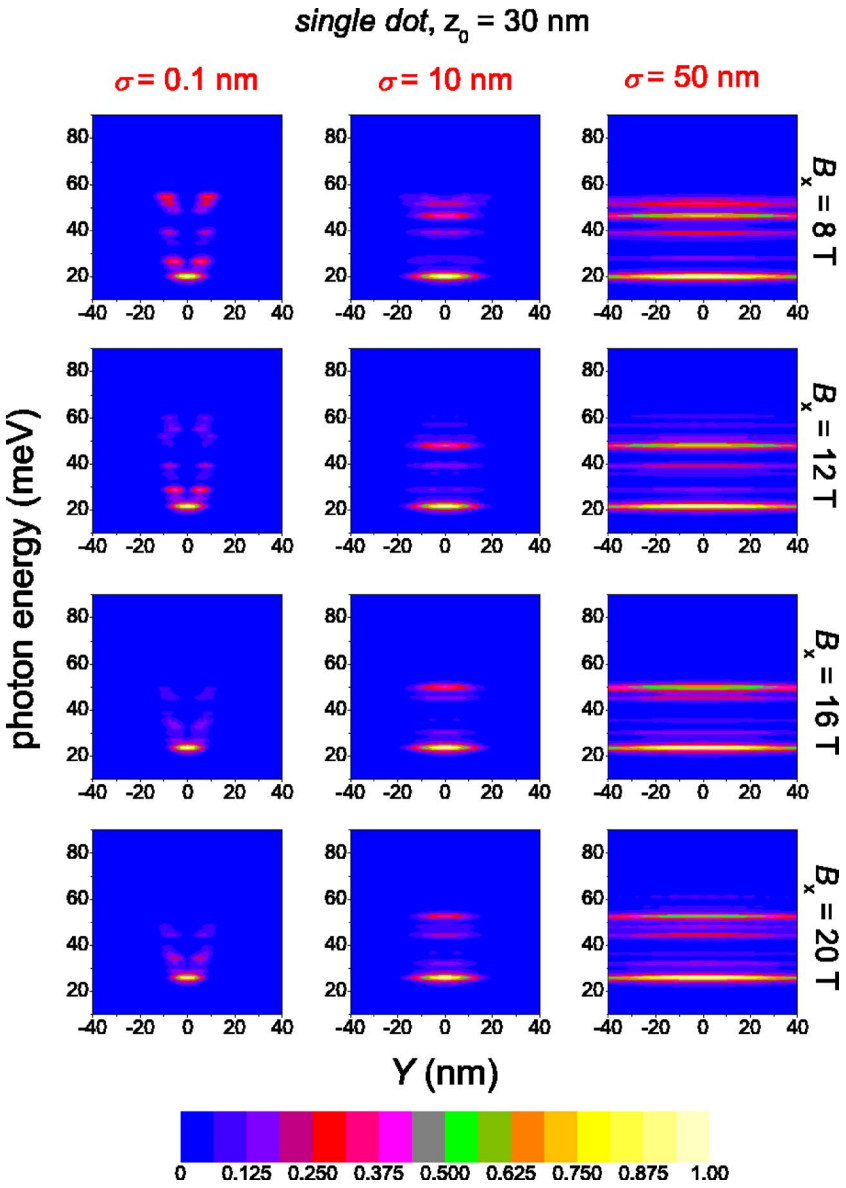

FIG. 7. (Color online) The same *single quantum dot* and magnetic field orientation with Fig. 6. Now $\alpha_\xi(Y,\hbar\omega)$ is illustrated, keeping $X=0$. The zero-magnetic-field "structural" cylindrical symmetry has been broken by the "in-plane" magnetic field. For this reason this Y scan ($X=0$) is not equivalent to the X scan ($Y=0$) illustrated in Fig. 6.

maximum (FWHM) of the Gaussian (i.e., $2\sqrt{2\ln 2}\sigma \approx 2.35\sigma$).[39]

III. RESULTS AND DISCUSSION

A. Single-particle states of single QDs: Spatial confinement vs magnetic field orientation and magnitude

To start with, we consider the geometry of a single QD with parabolic confinement (pc) in the xy plane and a square quantum well in the z axis.[22] In order to examine the relative influence of the spatial versus the magnetic confinement, we vary the QW width z_0. Specifically, we use the values $z_0=10$ nm, 20 nm, and 30 nm. The lateral dimension of the QDs (xy plane) is determined[22] by the confinement energy of electrons and holes which is taken $\hbar\omega_{pc}=20$ meV and 3.5 meV, respectively. The material parameters used here are appropriate for GaAs/AlGaAs QDs: In the z axis, we take 300 meV and 200 meV for the conduction-band and valence-band offsets, respectively. We use $0.067m_e$ and $0.38m_e$ (m_e is the electron mass) for the effective mass of electrons and holes, respectively, and everywhere 12.9 for the dielectric constant. Without application of a magnetic field, this system has cylindrical symmetry. The application of a magnetic field modifies the energy spectrum.

Under a "perpendicular" magnetic field applied in the z direction, the system is rotationally symmetric relative to the z axis; i.e., the QD retains its cylindrical symmetry. The total eigenenergies are given by $E_{xy}+E_z$. The z-axis eigenenergies are determined by the QW—i.e., $E_z=E_i$, where i is a natural number. Because of the parabolic confinement in the xy plane, application of a "perpendicular" magnetic field along the z axis changes the height of the energetic staircase and removes the degeneracy proportionally to B (Refs. 40 and 41); i.e., the xy plane eigenenergies become

$$E_{xy} = E_{n_\rho,m_l} = \hbar\Omega(2n_\rho + |m_l| + 1) \pm \hbar\omega_B m_l/2, \qquad (10)$$

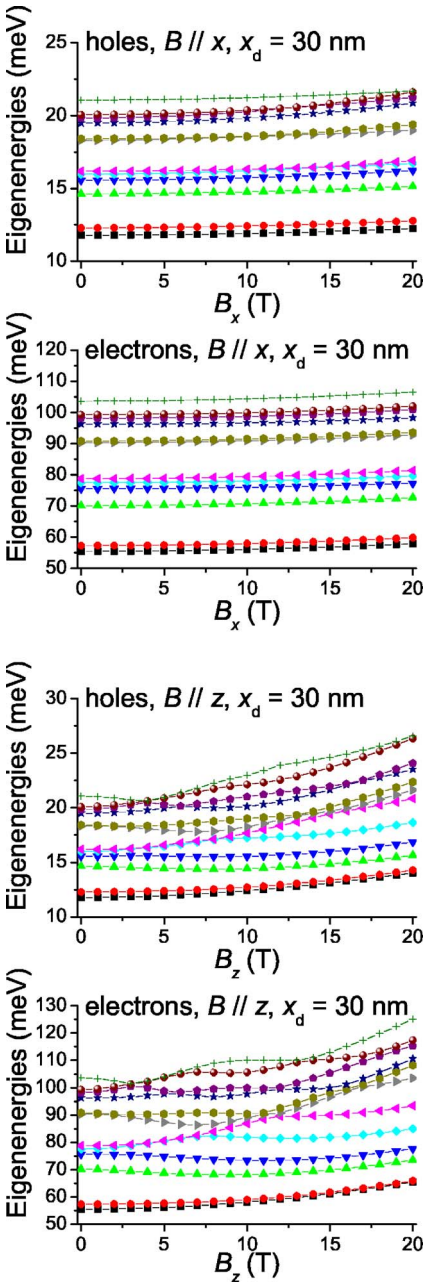

FIG. 8. (Color online) *Double quantum dot* with a soft barrier and interdot distance along x, $x_d=30$ nm. The QW width is $z_0=10$ nm and the confinement is parabolic along y. Single-particle hole and electron eigenenergies as a function of $\boldsymbol{B}$, applied in the x ($B\|x$) or in the z ($B\|z$) direction. Here twelve hole and twelve electron eigenenergies are presented.

$$\Omega^2 = \omega_B^2/4 + \omega_{pc}^2. \tag{11}$$

As mentioned above, the energy scale $\hbar\omega_{pc}$ stems from the "spatial" parabolic confinement in the xy plane. On the other hand, $\hbar\omega_B=\hbar eB/m^*$ is the cyclotron gap which is related to the "magnetic confinement." n_ρ is a natural number and m_l is an integer. In the following, the states with $n_\rho=0,1,2,\ldots$ are denoted as $1,2,3,\ldots$. The states with $m_l=0,\pm1,\pm2,\ldots$ are characterized as $s,p,d,\ldots$. Moreover, in Eq. (10), the plus (+) sign corresponds to electrons and the minus (−) sign to holes. Due to the rotational symmetry relative to the z axis under a "perpendicular" magnetic field, the z component of the angular momentum (with eigenvalues $\hbar m_l$) is conserved.

On the other hand, under an "in-plane" magnetic field, applied along the x or y axis, the symmetry of the system is broken; i.e., it is no longer cylindrical. This is a case where an analytical solution of the single-particle problem is not straightforward, a case underlining the power of the numerical procedure proposed in the present work. Under "in-plane" magnetic field, none of the components of the angular momentum is conserved. In any case, in analogy with QWs,[42] one would expect the influence of an "in-plane" magnetic field to increase with the QW width.

Figure 1 presents the single-particle eigenenergies as a function of the "in-plane" magnetic field applied along the x axis or as a function of the "perpendicular" magnetic field applied along the z axis for the QD with $z_0=10$ nm. For $B=0$, we have already postulated that the energetic separation of the degenerate groups of eigenstates is 3.5 meV for holes and 20 meV for electrons. For this *narrow* QW, for $B=0$, the energetic separation of the z-axis eigenenergies E_z is so large that we can distinguish the expansion of the first four groups of degenerate (for $B=0$) xy-plane eigenenergies E_{xy} into nondegenerate (for $B_z\neq0$) ones. The population of these first four groups is $1+2+3+4$ [cf. Eq. (10)], equal to the number of eigenstates chosen to be presented in Fig. 1. For $B=0$, a single E_{xyz} ladder, the corresponding to the ground state E_z, is depicted in Fig. 1. Hence, this QD with $z_0=10$ nm, under a "perpendicular" magnetic field, retains its cylindrical symmetry and a single E_{xyz} ladder for $B=0$. Henceforth, this will be referred as *ideal* configuration. Due to the very small QW width, as expected, the "in-plane" magnetic field negligibly affects the single-particle eigenstates. Therefore, for this QD with $z_0=10$ nm, discussing the absorption spectra, we will restrict ourselves to the case of the "perpendicular" magnetic field.

Figure 2 presents the single-particle eigenenergies as a function of the "in-plane" magnetic field applied along the x axis for the QDs with $z_0=20$ nm and 30 nm. For $B=0$, we have already postulated that the energetic separation of the degenerate groups of eigenstates is 3.5 meV for holes and 20 meV for electrons. Increasing the QW width, the spatial confinement diminishes. Hence, we observe an increasing influence of the magnetic confinement caused by the "in-plane" magnetic field. Moreover, as expected (for $B=0$),[43] increasing z_0, the energetic separation of the z-axis eigenenergies E_z decreases. Consequently, for $B=0$, more than one E_{xyz} ladder is depicted in Fig. 2. Relative to the case with $z_0=20$ nm, the mixing of the E_{xyz} ladders is enhanced for the QD with $z_0=30$ nm. Since under "in-plane" magnetic field the z axis is not anymore a symmetry axis, the symmetry is higher under "perpendicular" magnetic field. This is expected to be reflected upon the NF spectra.

B. Single QD in *ideal* configuration: The influence of the Coulomb interaction

Figure 3 depicts the magnetoabsorption spectra of our single QD with $z_0=10$ nm, in the *ideal* configuration, *taking*

TABLE I. All excitons with some FF-bright components, for $B_z=4$ T, in the energy range which includes all the 36 excitons of the $6e$-$6h$ description. The $10e$-$10h$ description provides two "new" such excitons, the ones with (the FF-dark) key components $1p(-1)$-$2p(+1)$ and $1p(+1)$-$2p(-1)$. All eigenenergies are quoted in meV. The asterisk (*) denotes an FF-bright and @ an FF-dark key component.

Key component	E^τ $6e$-$6h$	E^τ $10e$-$10h$	$\mathcal{C}^\tau_{key\ component}$ $6e$-$6h$	$\mathcal{C}^\tau_{key\ component}$ $10e$-$10h$
$1s(0)$-$1s(0)$*	51.9	51.7	(0.96,0.00)	(0.96,0.00)
$1s(0)$-$2s(0)$@	65.4	65.3	(0.96,0.00)	(0.96,0.00)
$1p(-1)$-$1p(+1)$*	77.1	76.8	(0.94,0.00)	(0.93,0.00)
$1p(+1)$-$1p(-1)$*	85.9	85.6	(0.96,0.00)	(0.95,0.00)
$1p(-1)$-$2p(+1)$@		87.3		(0.96,0.00)
$1p(+1)$-$2p(-1)$@		95.7		(0.95,0.00)
$2s(0)$-$1s(0)$@	98.4	98.1	(0.88,0.00)	(0.83,0.00)
$1d(-2)$-$1d(+2)$*	99.7	99.5	(0.87,0.00)	(0.80,0.00)
$2s(0)$-$2s(0)$*	107.7	107.5	(0.97,0.00)	(0.95,0.00)
$1d(+2)$-$1d(-2)$*	115.9	115.9	(0.98,0.00)	(0.98,0.00)

into account or *neglecting* the Coulomb interaction, for relatively small values of the "perpendicular" magnetic field ($B=0$, $B_z=1$ T, and $B_z=4$ T). The multipanel plots correspond to different radii, $2\sqrt{2\ln 2}\sigma \approx 2.35\sigma$, of the illuminated spot: (a) $\sigma=0.1$ nm, (b) $\sigma=10$ nm, and (c) $\sigma=50$ nm. Within each multipanel plot, each row corresponds to a different value of the magnetic field, while each column corresponds to results *with* or *without* Coulomb interactions. A normalized color code is used to illustrate the local absorption, $\alpha_\xi(X,\hbar\omega)$, as a function of the tip position along the x axis denoted by X, and the photon energy measured with respect to the band gap, $\hbar\omega$. The position of the tip along the y axis is kept $Y=0$. Due to the cylindrical symmetry of this configuration, any scan passing through the center of the dot would produce the same result. In Fig. 3, to facilitate the discussion, for the solution of the excitonic problem, we took into account six electron and six hole eigenstates ($6e$-$6h$ description). This number $(1+2+3)$ is equal to the first three groups of degenerate for $B=0$ eigenstates of electrons or holes [cf. Eq. (10)]. We have also performed calculations taking into account ten electron and ten hole eigenstates ($10e$-$10h$ description), which corresponds to the inclusion of the first four groups of degenerate for $B=0$ eigenstates of electrons or holes $(1+2+3+4)$. As expected, increasing the photon energy, the $10e$-$10h$ description deviates from the $6e$-$6h$ one. However, for low photon energies the two pictures almost coincide. Moreover, considering the excitons which possess some FF-bright components, the two pictures come even closer, in the energy range which includes all the 36 excitons of the $6e$-$6h$ picture. We will return to this point later on. An exemplary comparison of the two descriptions is presented in Table I. As expected, the Coulomb interaction leads to a nearly rigid redshift and transfers the oscillator's strength from higher to lower energies. We notice that, *for this QD*, for $\sigma=50$ nm the absorption spectra depend only slightly on the tip position; i.e., the "far-field" limit is almost reached. We also observe that for $B=0$, the Coulomb interaction is responsible for the appearance of an additional feature at ≈ 65 meV which is strong for $\sigma=0.1$ nm, almost disappears for $\sigma=10$ nm, and is again strong in the "far field." The intensity of such spectral features depends on the spatial resolution in a remarkably nonmonotonic way, presenting a minimum when the spatial resolution is close to ρ.[22] Here we notice that for $B_z=1$ T and 4 T, this feature at ≈ 65 meV not only retains but also strengthens this nonmonotonic behavior. For $B_z=4$ T, due to the slight modification of the relevant single-particle eigenenergies, this transition is slightly shifted to ≈ 65.4 meV. Moreover, for $B_z=4$ T, there are additional features (e.g., at $\approx 98-100$ meV) which demonstrate a rather nice "nonmonotonous" character, in the sense described above.

In order to depict the "far-field" transitions in a less glamorous but more precise fashion, we illustrate in Fig. 4 the "far-field" ($\sigma=50$ nm) spectra of Fig. 3, as a function of the photon energy only (i.e., for all tip positions X). Initially, we consider the results *without* Coulomb matrix elements. Since in the far-field regime $\alpha^\tau_\xi(\boldsymbol{R}) \propto |\int d^3\boldsymbol{r}\Psi^\tau(\boldsymbol{r},\boldsymbol{r})|^2$, only transitions between electron and hole single-particle states for which the z component of the total angular momentum is zero are FF allowed; i.e., the necessary rule is $m^e_l+m^h_l=0$. However, this rule is not sufficient. If the transition is to survive in the far field, the radial integral must also be nonzero. The removal of the degeneracy, caused by the "perpendicular" magnetic field, increases the number of FF-allowed transitions, from 3 ($B=0$) to 6 ($B_z=4$ T). For $B=0$, the energetically lowest transition is not degenerate, the next one is doubly degenerate, and the highest one is triply degenerate. For this reason, their oscillator strength follows quite precisely a 1:2:3 law. On the other hand, for $B_z=4$ T, due to the removal of the degeneracy, all transitions show approximately the same oscillator strength. The peak energies of all these transitions can be identified with the sum of the corresponding electron and hole single-particle eigenenergies, since we ignore the band gap in the presentation of our results. For $B_z=4$ T, in order of increasing energy, we distinguish the following transitions: $1s(m^e_l=0)$ to $1s(m^h_l=0)$, $1p(m^e_l=-1)$ to $1p(m^h_l=+1)$, $1p(m^e_l=+1)$ to $1p(m^h_l=-1)$ and $1d(m^e_l=-2)$ to $1d(m^h_l=+2)$, $2s(m^e_l=0)$ to $2s(m^h_l=0)$, $1d(m^e_l=+2)$ to $1d(m^h_l=-2)$. For $B=0$, the two ($1p$-$1p$) transitions are degenerate. For $B=0$, the two ($1d$-$1d$) transitions and the ($2s$-$2s$) transition are degenerate, too. In the following, we simplify the symbolism; e.g., for the transition $1d(m^e_l=+2)$ to $1d(m^h_l=-2)$, we write $1d(+2)$-$1d(-2)$.

The inclusion of the Coulomb interaction mixes the transitions between single-particle electron and hole states. The relative contribution of each single-particle electron- (μ-) hole (ν) transition to a particular exciton (τ) is given by Eq. (7). Generally, the increase of B_z to 4 T leads to a much more distinct character of the excitonic eigenstates, which mirrors the redistribution of the single-particle eigenstates (cf. Fig. 1). Table I quotes, in order of increasing energy, for $B_z=4$ T, the excitons which contain some FF-allowed single-particle electron- (μ-) hole (ν) transitions—i.e., FF-bright components. Table I also compares the $6e$-$6h$ to $10e$-$10h$ description, for $B_z=4$ T, in the energy range which embraces

all the 36 excitons of the $6e$-$6h$ description. Only excitons with at least one FF-bright component are listed—i.e., excitons with vanishing z component of the total angular momentum. The catalog includes the *key component* [the one with the dominant coefficient, $\mathcal{C}^{\tau}_{\mu\nu}$, in the expansion of Eq. (7)] and the exciton eigenenergy E^{τ}, as well as $\mathcal{C}^{\tau}_{key\ component}$. In the present energy range, the $10e$-$10h$ description provides only two "new" excitons with some FF-bright components: the ones with (the FF-dark) key components $1p(-1)$-$2p(+1)$ and $1p(+1)$-$2p(-1)$. Apart from this, the two descriptions are very similar in the energy range of interest, for the excitons with some FF-bright components. E^{τ} are in fact very close, with a maximum difference of 0.3 meV, while $\mathcal{C}^{\tau}_{key\ component}$ are almost identical as well, except for the excitons with key components $2s(0)$-$1s(0)$ and $1d(-2)$-$1d(+2)$. Actually, the exciton with key component $2s(0)$-$1s(0)$ has an important $1d(-2)$-$1d(+2)$ component and vice versa, and the little differences are due to the interplay between these two components.

C. Single QDs subjected to higher magnetic field

The application of a small perpendicular magnetic field was sufficient to remove the degeneracy, modifying the magnetoabsorption spectra. However, the spatial confinement still dominates for small values of the magnetic field. Below, in Secs. III C–III E, to evaluate the significance of the magnetic confinement, we increase B up to 20 T. Moreover, in Secs. III C and III E the magnetic field orientation is also varied in order to emphasize its importance.

Let us consider again our single QD in the *ideal* configuration. For $B_z > 4$ T, the range of the six energetically lowest electron or hole eigenstates—used in this exemplary calculation—is enriched with higher quantum numbers n_ρ and $|m_l|$, while simultaneously some of the states with lower quantum numbers move to higher energies and are therefore omitted from our calculation (cf. Fig. 1). In Fig. 5, we show the magnetoabsorption spectra of this configuration for higher values of B_z (8 T, 12 T, 16 T, and 20 T), for different spatial resolution, $2\sqrt{2\ln 2}\sigma \approx 2.35\sigma$ ($\sigma=0.1$ nm, $\sigma=10$ nm, and $\sigma=50$ nm), including the Coulomb interactions in the calculation. Specifically, the local absorption $\alpha_{\xi}(X,\hbar\omega)$ is presented, keeping $Y=0$. Each column corresponds to different spatial resolution, while each row corresponds to a different value of the "perpendicular" magnetic field. We observe that, due to the incessant rearrangement of the single-particle eigenstates, brought about by the increase of B_z, the number of FF-allowed excitons is continuously modified. We underline that the "structural" (for $B=0$) cylindrical symmetry is preserved here by the "perpendicular" magnetic field. Therefore, any scan passing through the center of the dot (e.g., along Y, keeping $X=0$) would produce the same result with the present scan.

Figure 6 demonstrates the absorption spectra of the QD with $z_0=30$ nm for relatively high values of B_x (8 T, 12 T, 16 T, and 20 T). Specifically, we show the local absorption $\alpha_{\xi}(X,\hbar\omega)$, keeping $Y=0$. Figure 6 is "the broken-symmetry counterpart" of Fig. 5: the zero-magnetic-field "structural" cylindrical symmetry has now been destroyed by the "in-plane" magnetic field. Therefore, different scans passing through the center of the dot are now not equivalent; e.g., this scan along X keeping $Y=0$ (cf. Fig. 6) is not equivalent to a scan along Y keeping $X=0$ (cf. Fig. 7). This asymmetry is still evident for $\sigma=10$ nm, but it is vanishing for $\sigma=50$ nm.[44] The comparison of Figs. 6 and 7 illustrates that the destruction of the symmetry (asymmetry) induced by the "in-plane" magnetic field can be revealed in the near-field but not in the far-field spectra.

Pushing our thoughts a little further, we anticipate that near-field magnetoabsorption experiments, of realistic spatial resolution, could be used to reveal the symmetry of QDs. If, for example, the QD is of "structural" cylindrical symmetry, as above, application of the magnetic field along the "structural" symmetry axis preserves the QD symmetry. Therefore, transverse scans in a plane perpendicular to $\boldsymbol{B}$ will produce equivalent near-field spectra. On the other hand, application of the magnetic field along another orientation will more or less destroy the QD "structural" symmetry. Therefore, the transverse scans will produce dissimilar near-field spectra. This impressive *symmetry-resolving power* of the near-field magnetoabsorption is lost in the far field.

The asymmetry which can be revealed in the NF but not in the FF spectra and the symmetry-resolving power of the NF magnetoabsorption, a property lost in the far field, are *characteristic* differences between the near-field and far-field magnetoabsorption.

D. Double QD with a soft barrier

Finally, we consider the geometry of a specific *double quantum dot*. Namely, there is a parabolic confinement along the y axis and a square QW along the z axis, while for the x axis, the potential energy has two minima separated by a prototype[22] soft barrier. The interdot distance—i.e., the separation of the two minima—is taken $x_d=30$ nm. The QW width $z_0=10$ nm. All other material parameters are the same with the ones used above. Figure 8 presents the single-particle eigenenergies of this prototype double QD as a function of $\boldsymbol{B}$, applied in the x or z direction.

Figure 9 illustrates the effect of a strong magnetic field on the NF absorption spectra of this double QD. The two rows correspond to $\sigma=0.1$ nm and $\sigma=10$ nm. The two columns correspond to $B=0$ and $B_z=20$ T. In this example, for the solution of the excitonic problem, we use a basis of twelve electron and twelve hole states. Due to the relatively soft confinement along x, we observe that the strong magnetic field leads to much more "confined" excitons. In other words, for $B_z=20$ T, the spatial extent of the excitonic wave functions has been decreased by $\approx 1/3$, while there is a considerable blueshift of the excitonic eigenspectrum. It is in our opinion important to realize that such modifications of the excitonic structure can indeed be exposed via a realistically acute near-field probe with a spatial resolution of $2\sqrt{2\ln 2}\times 10\ \text{nm} \approx 2.35\times 10\ \text{nm} = 23.5$ nm.

E. Ground-state exciton binding

The spatial confinement as well as $\boldsymbol{B}$ (magnitude and orientation) influences the single-particle electron and hole

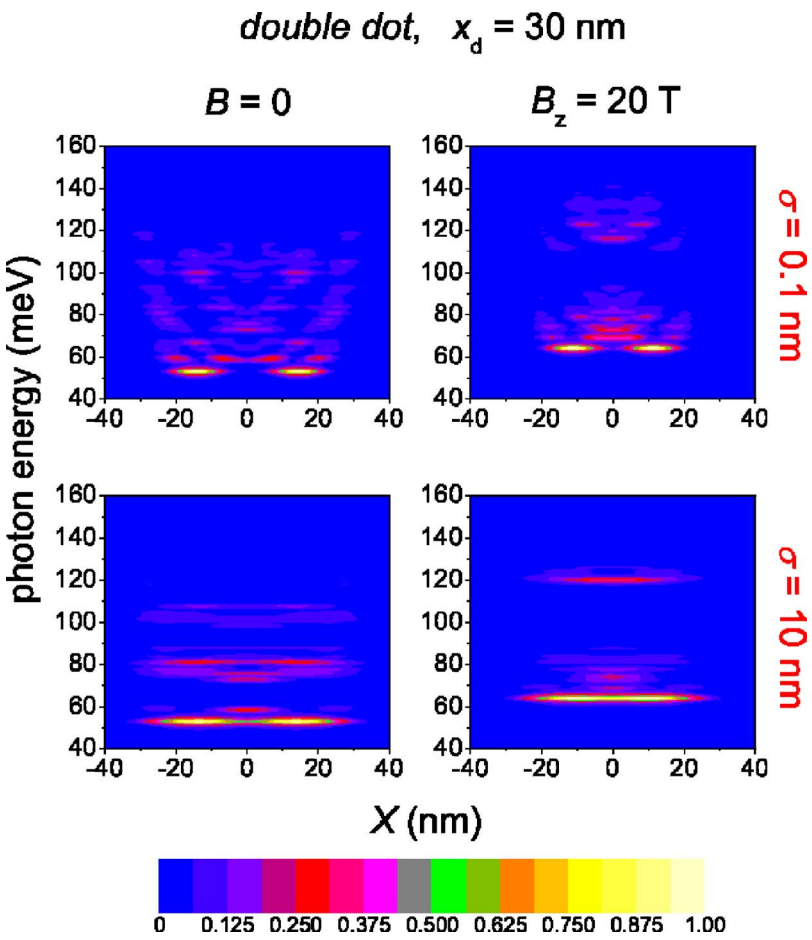

FIG. 9. (Color online) *Double quantum dot* with a soft barrier and interdot distance along x, x_d=30 nm. The QW width is z_0=10 nm and the confinement is parabolic along y. Local absorption $\alpha_\xi(X,\hbar\omega)$ (color scale) as a function of the tip position along the x axis, X (nm), and the photon energy measured with respect to the band gap, $\hbar\omega$ (meV). We keep Y=0. Each row corresponds to different spatial resolution $2\sqrt{2\ln 2}\sigma \approx 2.35\sigma$: σ=0.1 nm and σ=10 nm. Each column corresponds to a different value of the magnetic field—i.e., B=0 and B_z=20 T.

eigenenergies (cf. Figs. 1 and 2). Moreover, the spatial confinement and $\boldsymbol{B}$ influence the Coulomb interaction, which in its turn affects the exciton eigenenergies. This obviously offers a way to engineer the ground-state exciton binding energy $E_b=E_e+E_h-E_{xc}$. Here E_e (E_h) is the ground-state electron (hole) eigenenergy and E_{xc} is the ground-state exciton eigenenergy. Figure 10 depicts E_b as a function of the magnetic field applied along the x or z axis for the four characteristic cases of spatial confinement as well as magnetic confinement and orientation described in Figs. 1 and 2 (z_0 =10 nm and $\boldsymbol{B}$ along x, z_0=10 nm and $\boldsymbol{B}$ along z, z_0 =20 nm and $\boldsymbol{B}$ along x, z_0=30 nm and $\boldsymbol{B}$ along x). We observe that for B=0, the size of the QD determines the magnitude of E_b. The electrons and holes which are confined in a smaller QD interact more effectively, and accordingly this leads to a higher E_b. Increasing B, the magnetic confinement brings even closer electrons and holes, and consequently E_b increases. As expected, for the very narrow QD, the in-plane magnetic field has a negligible effect on E_b.

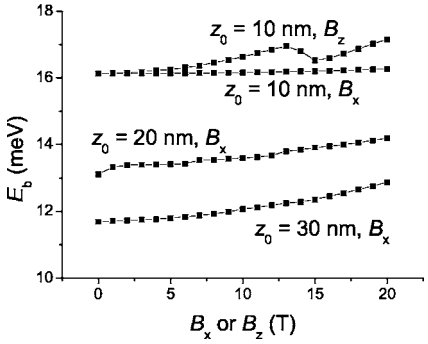

FIG. 10. The ground-state exciton binding energy E_b as a function of the magnetic field applied along the x or z axis for the four characteristic cases depicted in Figs. 1 and 2.

Large E_b relative to the thermal energy, $k_BT_{room} \approx 26$ meV, is certainly desirable because it is necessary for optical devices able to operate efficiently at room temperature. We observe that a way to increase E_b is by "squeezing" the electron and hole wave functions—i.e., by choosing smaller QDs or by increasing B, thereby forcing the single-particle carriers to get closer. However, this "squeezing" depends also on the band offsets (GaAs/AlGaAs in our calculations) which are certainly finite. Moreover, decreasing z_0, the single-particle wave functions start to penetrate into the AlGaAs barrier. Rossi *et al.* have shown that, generally, compared to QWs, larger E_b can be achieved in QWRs, but for all GaAs-based QWRs considered, they found $E_b < k_BT_{room}$.[45] We notice that our combination of *spatial* and *magnetic* confinement leads to E_b close to k_BT_{room}. To further increase E_b, with the aim of achieving room-temperature exciton binding, one could, e.g., additionally employ *remote dielectric* confinement as already suggested for QWRs (Ref. 46)—i.e., exploit the confinement induced by the dielectric mismatch[47] of remotely placed oxide layers.

IV. CONCLUSION

We presented a theoretical framework for the investigation of the linear near-field absorption spectra of semiconductor quantum dots under magnetic field of variable orientation and magnitude. We examined the influence of the *spatial* as well as of the *magnetic* confinement. This offers a way to manipulate the excitonic structure—e.g., the ground-state exciton binding energy. The magnetic field *orientation* was shown to be an important factor. The application of the magnetic field reorganizes the single-particle hole and electron eigenstates. This, along with the concomitant amendment of the Coulomb interactions, induces a plethora of modifications to the NF spectra. It was shown that realistically acute up-to-date NF probes can actually bring to light (sic) some of these modifications. Depending on its orientation, the magnetic field can *preserve* or *destroy* the "structural" zero-magnetic-field symmetry. The asymmetry induced by the magnetic field (except for specific orientations along structural symmetry axes) can be revealed in the NF but not in the FF spectra. Moreover, we demonstrated that near-field magnetoabsorption experiments, of realistic spatial resolution, will enable us to reveal the symmetry of QDs. This impressive *symmetry-resolving power* of the near-field magnetoabsorption is lost in the far field. The asymmetry which can be revealed in the NF but not in the FF spectra and the symmetry-resolving power of the NF magnetoabsorption, a property lost in the far field, are *characteristic* differences between the near-field and far-field magnetoabsorption. Finally we notice that inclusion of a more accurate description of holes away from the single-band simplifying hypothesis, as well as of the spin, will lead to a more accurate appreciation of the above-mentioned modifications.

ACKNOWLEDGMENTS

We thank Ulrich Hohenester for his comments. This work was supported in part by the Hellenic Ministry of Education under the program "Heracletus."

*Corresponding author. Electronic address: csimseri@phys.uoa.gr, URL: http://users.uoa.gr/~csimseri/

[1] E. H. Synge, Philos. Mag. **6**, 356 (1928).
[2] U. Durig, D. W. Pohl, and F. Rohner, J. Appl. Phys. **59**, 3318 (1986).
[3] J. M. Vigoureux and D. Courjon, Appl. Opt. **31**, 3170 (1992).
[4] E. A. Ash and G. Nicholls, Nature (London) **237**, 510 (1972).
[5] A. Lewis, M. Isaacson, A. Harootunian, and A. Muray, Biophys. J. **41**, 405 (1983); Ultramicroscopy **13**, 227 (1984).
[6] D. W. Pohl, W. Denk, and M. Lanz, Appl. Phys. Lett. **44**, 651 (1984).
[7] J. R. Guest, T. H. Stievater, G. Chen, E. A. Tabak, B. G. Orr, D. G. Steel, D. Gammon, and D. S. Katzer, Science **293**, 2224 (2001).
[8] J. Hwang, L. K. Tamm, C. Böhm, T. S. Ramalingam, E. Betzig, and M. Edidin, Science **270**, 610 (1995).
[9] B. Knoll and F. Keilmann, Nature (London) **399**, 134 (1999).
[10] J. K. Trautman, J. J. Macklin, L. E. Brus, and E. Betzig, Nature (London) **369**, 40 (1994).
[11] C. L. Jahncke, M. A. Paesler, and H. D. Hallen, Appl. Phys. Lett. **67**, 2483 (1995).
[12] S. K. Buratto, J. W. P. Hsu, E. Betzig, J. K. Trautman, R. B. Bylsma, C. C. Bahr, and M. J. Cardillo, Appl. Phys. Lett. **65**, 2654 (1994).
[13] S. Madsen, S. I. Bozhevolnyi, K. Birkelund, M. Müllenborn, J. M. Hvam, and F. Grey, J. Appl. Phys. **82**, 49 (1997).
[14] U. Hartmann, J. Magn. Magn. Mater. **157-158**, 545 (1996).
[15] S. Sangu, K. Kobayashi, A. Shojiguchi, and M. Ohtsu, Phys. Rev. B **69**, 115334 (2004).
[16] A. Lewis, H. Taha, A. Strinkovski, A. Manevitch, A. Khatchatouriants, R. Dekhter, and E. Ammann, Nat. Biotechnol. **21**, 1378 (2003).
[17] B. Hecht, B. Sick, U. P. Wild, V. Deckert, R. Zenobi, O. J. F. Martin, and D. W. Pohl, J. Chem. Phys. **112**, 7761 (2000).
[18] D. Courjon and C. Bainier, Rep. Prog. Phys. **57**, 989 (1994).
[19] C. Girard and A. Dereux, Rep. Prog. Phys. **59**, 657 (1996).
[20] C. Girard, C. Joachim, and S. Gauthier, Rep. Prog. Phys. **63**, 893 (2000).
[21] O. Mauritz, G. Goldoni, F. Rossi, and E. Molinari, Phys. Rev. Lett. **82**, 847 (1999).
[22] C. D. Simserides, U. Hohenester, G. Goldoni, and E. Molinari, Phys. Rev. B **62**, 13657 (2000).
[23] C. D. Simserides, U. Hohenester, G. Goldoni, and E. Molinari, in *Proceedings of the International Conference on Semiconductor Quantum Dots, Münich, 2000*, edited by U. Woggon and A. Zrenner [Phys. Status Solidi B **224**, 745 (2001)] (Wiley-VCH Verlag, Berlin, 2001).
[24] E. Betzig, J. K. Trautman, T. D. Harris, J. S. Weiner, and R. L. Kostelak, Science **251**, 1468 (1991).
[25] K. Matsuda, T. Saiki, S. Nomura, M. Mihara, and Y. Aoyagi, Appl. Phys. Lett. **81**, 2291 (2002).
[26] K. Matsuda, T. Saiki, S. Nomura, M. Mihara, Y. Aoyagi, S. Nair, and T. Takagahara, Phys. Rev. Lett. **91**, 177401 (2003).
[27] U. Hohenester, G. Goldoni, and E. Molinari, Appl. Phys. Lett. **84**, 3963 (2004).
[28] E. Runge and C. Lienau, Phys. Rev. B **71**, 035347 (2005).
[29] U. Hohenester, G. Goldoni, and E. Molinari, Phys. Rev. Lett. **95**, 216802 (2005).
[30] O. Mauritz, G. Goldoni, E. Molinari, and F. Rossi, Phys. Rev. B **62**, 8204 (2000).
[31] Initially shown by T. Ogawa and T. Takagahara, Phys. Rev. B **43**, R14325 (1991); **44**, 8138 (1991), who investigated the optical absorption and the Sommerfeld factors, and confirmed for realistic QWRs by F. Rossi and E. Molinari, Phys. Rev. Lett. **76**, 3642 (1996); Phys. Rev. B **53**, 16462 (1996), who—employing a density-matrix-based approach—also showed that the quenching holds in the linear as well as in the gain regime.
[32] S.-J. Cheng, W. Sheng, and P. Hawrylak, Phys. Rev. B **68**, 235330 (2003).
[33] P. Pereyra and S. E. Ulloa, Phys. Rev. B **61**, 2128 (2000).
[34] K. L. Janssens, F. M. Peeters, and V. A. Schweigert, Phys. Rev. B **63**, 205311 (2001).

[35] Manuel Valín-Rodríguez, Antonio Puente, and Llorenç Serra, Phys. Rev. B **64**, 205307 (2001).

[36] A. Zora, C. Simserides, and G. Triberis (unpublished).

[37] W. Sheng, S.-J. Cheng, and P. Hawrylak, Phys. Rev. B **71**, 035316 (2005).

[38] As discussed in the past (Ref. 22), in the far-field regime, where the electric field is spatially homogeneous, the oscillator strength α_ξ^τ is proportional to the spatial average of the excitonic wave function—i.e., $\alpha_\xi^\tau(\boldsymbol{R}) \propto \left|\int d^3\boldsymbol{r}\Psi^\tau(\boldsymbol{r},\boldsymbol{r})\right|^2$. In the opposite limit of an infinitely acute probe, $\xi(\boldsymbol{r}-\boldsymbol{R})=\delta(\boldsymbol{r}-\boldsymbol{R})$ and, consequently, $\alpha_\xi^\tau(\boldsymbol{R})=\left|\Psi^\tau(\boldsymbol{R},\boldsymbol{R})\right|^2$.

[39] Throughout this article we use $\sigma=50$ nm, $\sigma=10$ nm, or $\sigma=0.1$ nm. Calculations performed in this latter regime can be used to obtain a "cartography" of the exciton wave functions.

[40] V. Fock, Z. Phys. **47**, 446 (1928).

[41] C. G. Darwin, Proc. Cambridge Philos. Soc. **27**, 86 (1930).

[42] C. Simserides, J. Comput. Electron. **2**, 459 (2003); Phys. Rev. B **69**, 113302 (2004).

[43] See, e.g., G. Bastard, *Wave Mechanics Applied to Semiconductor Heterostructures* (Les éditions de physique, Paris, 1988).

[44] Careful inspection of Figs. 6 and 7 shows that for this larger QD the "far-field" limit has not been completely reached for $\sigma=50$ nm; i.e., some of the spectral features still depend on $\boldsymbol{R}$.

[45] F. Rossi, G. Goldoni, and E. Molinari, Phys. Rev. Lett. **78**, 3527 (1997).

[46] G. Goldoni, F. Rossi, and E. Molinari, Phys. Rev. Lett. **80**, 4995 (1998); F. Rossi, G. Goldoni, O. Mauritz, and E. Molinari, J. Phys.: Condens. Matter **11**, 5969 (1999).

[47] L. V. Keldysh, Pis'ma Zh. Eksp. Teor. Fiz. **29**, 716 (1979) [JETP Lett. **29**, 658 (1979)].